Phase Congruency Based on Derivatives of Gaussian Function: An Efficient Feature Map for Image Quality Assessment

Congmin Chen
Xi'an Jiaotong University https://orcid.org/0000-0002-9301-3892
Xuanqin Mou (xqmou@mail.xjtu.edu.cn)

Research

Keywords: Image quality assessment, full-reference, phase congruency, gradient magnitude, Laplacian of Gaussian

Posted Date: May 17th, 2022

DOI: https://doi.org/10.21203/rs.3.rs-1630821/v1

Phase Congruency Based on Derivatives of Gaussian Function: An Efficient Feature Map for Image Quality Assessment

Congmin Chen* and Xuanqin Mou**

*E-mail: chencongmin@stu.xjtu.edu.cn

** E-mail: xqmou@mail.xjtu.edu.cn (Corresponding author)

Institute of Image Processing and Pattern Recognition, Xi'an Jiaotong University, Xi'an, China, 710049.

Abstract

Image quality assessment (IQA) has become a hot issue in image processing, which aims to evaluate the quality of images automatically by a metric being consistent with subjective evaluations. Though deep learning based techniques have been applied to IQA models to achieve much progress, conventional IQA models that adopt deliberately designed features are still meaningful because by which we can learn what features are quality-aware and hence understand more about the way we improve image quality by enhancing quality-aware features. The first stage of conventional IQA model design is the quality-aware feature selection. Phase congruency (PC), as one of efficient saliency maps, which takes advantages of early visual feature, operates in frequency domain to measure local structure such as edges, corners, lines, etc. by computing the local amplitude and local energy in multiple scales. Conventional local PC feature is calculated with log-Gabor based filtration in several orientations, and is usually combined with other features in quality estimating. Recently, researchers suggested that spatially circular symmetric filters, such as gradient magnitude (GM) and Laplacian of Gaussian (LoG), are highly-efficient quality features that have been widely used in various IQA model designs. By considering the first-order derivative property of GM and the second-order derivative property of LoG, the two features are a suitable pairs for PC compositions while keeping the circular symmetric characteristic. Therefore, we use GM and LoG to construct a novel PC feature map and only use this feature map to build a full-reference (FR) IQA model, which is proved to be state-of-the-art on three benchmark databases. Furthermore, we replace the PC algorithm in the state-of-the-art FSIM metric with our PC computation, which achieves improved performance. This study suggests that the proposed circular symmetric PC feature is a high efficient quality feature and can be exclusively used in IQA model designs.

Keywords: Image quality assessment, full-reference, phase congruency, gradient magnitude, Laplacian of Gaussian.

1. Introduction

With the rapid growth of the technologies in digital communications and multimedia applications, more and more image data are produced for human observations. Human visual system (HVS) is the ultimate observer to judge the image quality. In order to improve efficiency, it is necessary to evaluate the quality of images automatically with a critical metric for different systems. Image quality assessment (IQA) aims at estimating the objective quality of images as closely to subjective judgements as possible, by means of establishing models. Among different IQA algorithms, full-reference (FR) IQA works when the original reference image is completely provided, no-reference (NR) is employed when the pristine reference image is not available, and reduced-reference (RR) works at the situation where partial information of reference image is provided. This paper focuses on FR-IQA methods, which are widely applied in estimating the image quality when reference image is considered to be perfect.

Conventional FR-IQA metrics such as mean squared error (MSE) and the peak signal-to-noise ratio (PSNR), which compute specific indicators on the intensity domain, evaluate the distortion degree by an arithmetic difference between reference and distorted images. The structural similarity (SSIM) index [1] is able to capture structural information when evaluating the image

quality on the basis of the assumption that the HVS is sensitive to local structures of visual signals. Based on that, the multi-scale SSIM (MS-SSIM) metric [2], with an extension to single-scale algorithm, calculates the brightness at the original scale, and compute the contrast and structural similarity at five scales altogether. Another variant of SSIM is the information weighted SSIM (IW-SSIM) metric [3], in which different types of local regions are considered to make different contributions to the quality of an image. Riesz transforms based feature similarity (RFSIM) [4] and spectral residual based similarity (SR-SIM) [5] metrics are also improvements which are computed on the basis of SSIM algorithm. Based on the statistical characteristics of natural images, the information fidelity criterion (IFC) [6] was proposed using the information theory. IFC evaluates the image quality by computing how much the original information is preserved in the distorted image compared with the reference image, and was upgraded to more efficient metric named visual information fidelity (VIF) [7]. Based on the fact that the HVS understands an image on its low-level features such as edges and zero-crossings [8-10] since the visual information is often redundant, a feature similarity (FSIM) index [11] measures the local structure by the value of phase congruency (PC). Based on the ability to convey local structure information, the image gradient is applied to evaluate the distortion of images. The gradient similarity (GSM) algorithm [12] measures the change in contrast and structure between reference and distorted images, and the gradient magnitude similarity deviation (GMSD) [13] makes use of the variation of gradient based local quality map. Another method to measure local structure of visual signal is to employ the Laplacian of Gaussian (LoG) filter, which is proved to be approximate to the de-correlating mechanism of the retinal ganglion receptive field in HVS [14, 15]. Non-shift edge based ratio (NSER) [16] makes use of early vision features produced by LoG filters, which are quality aware in representing structural distortions. More related researches prove that LoG is highly efficient in FR [17, 18], RR [19-21], and blind IQA [22] model design. In these related studies, LoG resembles the response of retinal ganglion receptive filed in HVS, and shows ability to retain structural distortions in all directions because of its circularly symmetric property. Especially, the joint distribution of GM and LoG in [22] has been proved to be efficient in IQA feature expressing and model design, and the relationship between GM and LoG has been explored for the first time. Since the non-directional filters are proved to be quality aware, GM and LoG generated from Gaussian function on the same scale are more universal in theoretical calculation and subsequent optimization in IQA related applications. Comprehensive surveys and detailed comparisons of modern IQA metrics are discussed in many literatures [23-26].

Aside from conventional IQA methods, convolutional neural networks (CNN) have been applied to IQA issues in recent researches [27-29]. Generally, the networks indicate perceptual distortions by multilayer convolution structures, followed by an aggregation or pooling step. Although existing CNNs have reached good performance in predicting distortions, the generalization ability is difficult to improve in different situations due to the insufficiency of training data. Thus, studies on methodologies without training is still meaningful in practical applications. On the other hand, quality aware feature maps have also been employed as similarity maps [30] and quality aware loss [31] which helps to predict the discrepancy map. Therefore, quality aware

feature design is still a valuable issue in the related field.

As one of the most important components in visual signal processing, phase information carries more structural information than the spectral amplitude does in an image [32], low-level features such as edges and corners show consistence in phase according to Fourier translation. Based on physiological and psychophysical evidences, the PC theory provides a simple but biologically plausible model of how mammalian visual systems detect and identify features in an image [33-35]. The experiment based on the odd and even symmetry of visual receptive fields [33] explains that it is an efficient means for the visual system to locate the edges by the sum of the squared output of even and odd symmetric filters that always peaks at points of phase congruence. As the result, points of high PC value represent highly informative features. As a dimensionless index, conventional PC algorithm was defined by Morrone et al. in 1986 [33] and was developed by Kovesi [36, 37] based on a local energy model, which assumed that features are more evidently perceived at points where the Fourier components are maximally in phase. Many scholars have made use of PC features in IQA model design, where the computation is operated in frequency domain after filtration with multi-orientations, and have achieved good results. The phase-based algorithms usually employ the 2D Discrete Fourier Transform (DFT), Gabor filters [38], or log-Gabor filters [39] to calculate the phase information, which provides the ability to detect features from low quality images [40]. FSIM algorithm [11] combined PC with gradient magnitude, which is computed as the secondary feature to encode contrast information. [41] combined GM and local binary pattern (LBP) in PC domain at multiple scales to design the NR-IQA method with training a support vector regression model. A recent proposed metric based on symmetry phase congruency (SPCM) [42] also combined PC with GM in similarity computation.

In general, all PC based metrics for IQA model design use the even-symmetric and odd-symmetric components of the log-Gabor filters in multi-directions, for example, the filter in four orientations on four scales employed in FSIM index [11], and are always combined with other edge features. However, directional filters are more sensitive to structural distortions in specific directions. Meanwhile, it would increase the computational complexity and occupy more computing resources if more directions are retained in the filter banks. This motivated us to design a new term of PC computing method with consideration of non-directional filtration, and to build an IQA model using the PC features with lower computational complexity. As is well known, gradient filter is the first-order derivative of Gaussian filter, and LoG filter is the second-order derivative of Gaussian. As introduced in the previous paragraphs of this chapter, GM and LoG are quality aware features in IQA tasks, and are both generated from circular symmetric Gaussian function. It is obvious that gradient filter is an odd-symmetric filter, while LoG filter is an even-symmetric one. Therefore, we can use GM to represent the odd-symmetric components of an image, and LoG to the even-symmetric components. We utilized GM and LoG map for PC computing to obtain a non-directional PC operator. By calculating the similarity of PC map directly, we built a novel FR-IQA model, which is proved to be state-of-the-art compared with the competitors. Furthermore, we replaced the PC algorithm in FSIM with our PC computation method to test the ability of the proposed method to represent phase information,

and the experimental results revealed that the proposed PC feature map is able to correctly take the place of conventional PC algorithm.

The rest of this paper is organized as follows. Firstly, the computation of our proposed phase congruency method and a new FR-IQA metric are introduced in Section 2. Then in Section 3, experimental setups, results and comparisons on three benchmark databases are presented. Finally, Section 4 concludes the entire paper.

2. Methods

2.1 Phase congruency

The phase congruency (PC), which is a dimensionless quantity, was first proposed as a frequency based algorithm 33 instead of spatially processing on images. The basic concept of PC algorithm is that the Fourier components are maximal in phase where the local structure is perceived in an image. According to the extensively used PC algorithm, which was developed by Kovesi in [36], we consider a one-dimensional signal $f(x)$, and denote the even-symmetric filter and the odd-symmetric filter by M_n^e and M_n^o separately on scale *n*. We define a vector to represent the responses of the signal $f(x)$ after filtering by M_n^e and M_n^o on scale *n* as follows:

$$[e_n(x),\ o_n(x)] = [f(x) * M_n^e,\ f(x) * M_n^o] \tag{1}$$

where $e_n(x)$ and $o_n(x)$ are the output of M_n^e and M_n^o filtering at position *x*. The local amplitude on scale *n* is defined as:

$$A_n(x) = \sqrt{e_n(x)^2 + o_n(x)^2} \tag{2}$$

The local energy function can be written as:

$$E(x) = \sqrt{F^2(x) + H^2(x)} \tag{3}$$

where

$$F(x) = \sum_n e_n(x) \tag{4}$$

$$H(x) = \sum_n o_n(x) \tag{5}$$

The PC of one-dimensional signal is defined as:

$$PC(x) = \frac{E(x)}{\varepsilon + \sum_n A_n(x)} \tag{6}$$

where ε is a small positive constant to prevent the denominator from being zero.

Different from conventional methods, we apply the GM and LoG filters, which are the first-order and the second-order derivatives of Gaussian filter, instead of the log-Gabor based directional filters M_n^o and M_n^e. As shown in Figure 1, the normalized first-order and second-order derivatives of 1D Gaussian function are odd-symmetric and even-symmetric, respectively.

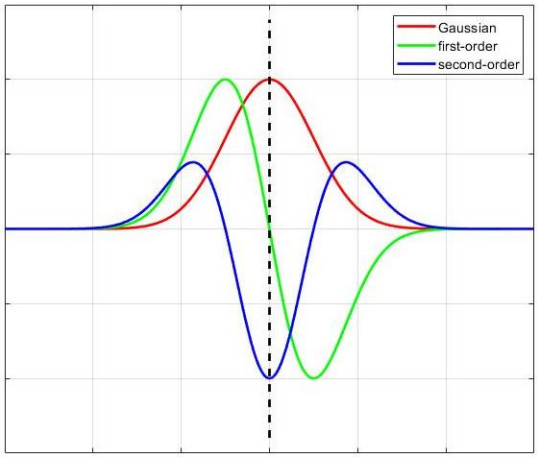

Figure 1. The first-order and second-order derivatives of 1D Gaussian function after normalization. The first-order derivate of Gaussian is an odd-symmetric filter that can generate signal gradient, and the second-order derivate of Gaussian is an even-symmetric filter, which is an LoG filter.

For 2D signals, the image gradient magnitude, which is defined as the root mean square of image directional gradients along two orthogonal directions, is still the first-order derivative of 2D Gaussian filter. We denote the Gaussian function by G, then the gradient filter on horizontal direction and vertical direction are defined as:

$$\boldsymbol{h}_x(x,y|\sigma) = (-\frac{1}{2\pi\sigma^4})xe^{-\frac{x^2+y^2}{2\sigma^2}} \tag{7}$$

$$\boldsymbol{h}_y(x,y|\sigma) = (-\frac{1}{2\pi\sigma^4})xe^{-\frac{x^2+y^2}{2\sigma^2}} \tag{8}$$

where the variables x and y denote the coordinate of the input image, parameter σ denotes the scale factor of the Gaussian function. We denote an image by $\boldsymbol{I}$, and convolve the image with the two directional derivative filters to produce the horizontal and vertical gradient images $\boldsymbol{d}_{n,x}$ and $\boldsymbol{d}_{n,y}$ on scale n, thus the GM of an image is computed as:

$$\begin{aligned} D_n(x,y) &= \sqrt{\boldsymbol{d}_{n,x}^2 + \boldsymbol{d}_{n,y}^2} \\ &= \sqrt{(\boldsymbol{I}\otimes\boldsymbol{h}_x)^2 + (\boldsymbol{I}\otimes\boldsymbol{h}_y)^2} \end{aligned} \tag{9}$$

The LoG filter, which is the second-order derivative of 2D Gaussian function, is defined as:

$$\boldsymbol{h}_{LOG}(x,y|\sigma) = -\frac{1}{\pi\sigma^4}(1-\frac{x^2+y^2}{2\sigma^2})e^{-\frac{x^2+y^2}{2\sigma^2}} \tag{10}$$

where the variables x and y denote the coordinate of the input image, parameter σ denotes the scale factor of the Gaussian function. Thus, the LoG map on scale n can be computed as:

$$L_n(x,y) = \boldsymbol{I} \otimes \boldsymbol{h}_{LOG} \tag{11}$$

In order to remove the contrast variation in the image of a large scale, we use divisive normalization 17 as:

$$V_n(x,y) = \frac{D_n(x,y)}{\sqrt{G_n(x,y) * D_n^2(x,y)} + c_0} \tag{12}$$

$$U_n(x,y) = \frac{L_n(x,y)}{\sqrt{G_n(x,y) * L_n^2(x,y)} + c_0} \tag{13}$$

where c_0 is a positive constant to ensure the stability of calculation, and $G_n(x,y)$ represents a large scale Gaussian filter employed for each scale *n*.

Therefore, the 2D local amplitude and local energy on scale n can be written as:

$$A_n(x,y) = \sqrt{U_n(x,y)^2 + V_n(x,y)^2} \tag{14}$$

$$E(x,y) = \sqrt{F^2(x,y) + H^2(x,y)} \tag{15}$$

where

$$F(x,y) = \sum_n U_n(x,y) \tag{16}$$

$$H(x,y) = \sum_n V_n(x,y) \tag{17}$$

Thus the PC can be computed by:

$$PC(x,y) = \frac{E(x,y)}{\varepsilon + \sum_n A_n(x,y)} \tag{18}$$

The value of PC ranges from 0 to 1, according to the definition, which tells that the value 0 means no significance whereas the value 1 means the most important feature. A higher value of PC means more significant the features which are perceived and more salient the edge that is being detected. Therefore, the PC map constructed from the odd-symmetric and the even-symmetric components can reflect the structural information of an image.

An analysis of the GM and LoG responses for different types of edge signals and distorted edges is shown in Fig. 2. In the first column, a pristine 1-D edge signal, a Gaussian blurred version, a Gaussian noise corrupted signal, and a DCT compressed signal are demonstrated from Figure 2(a) to Figure 2(d), respectively. The next two columns are the corresponding GM and LoG responses on two different scales. The last column shows the phase congruency curve computed by GM and LoG responses. The result validated that the proposed PC feature gives the highest value at the edge position for both original ideal edge and the corresponding distorted version, no matter which type of edge is to be processed. Based on this property, the proposed PC feature is suggested to have the ability to reflect the structural information of reference and distorted images.

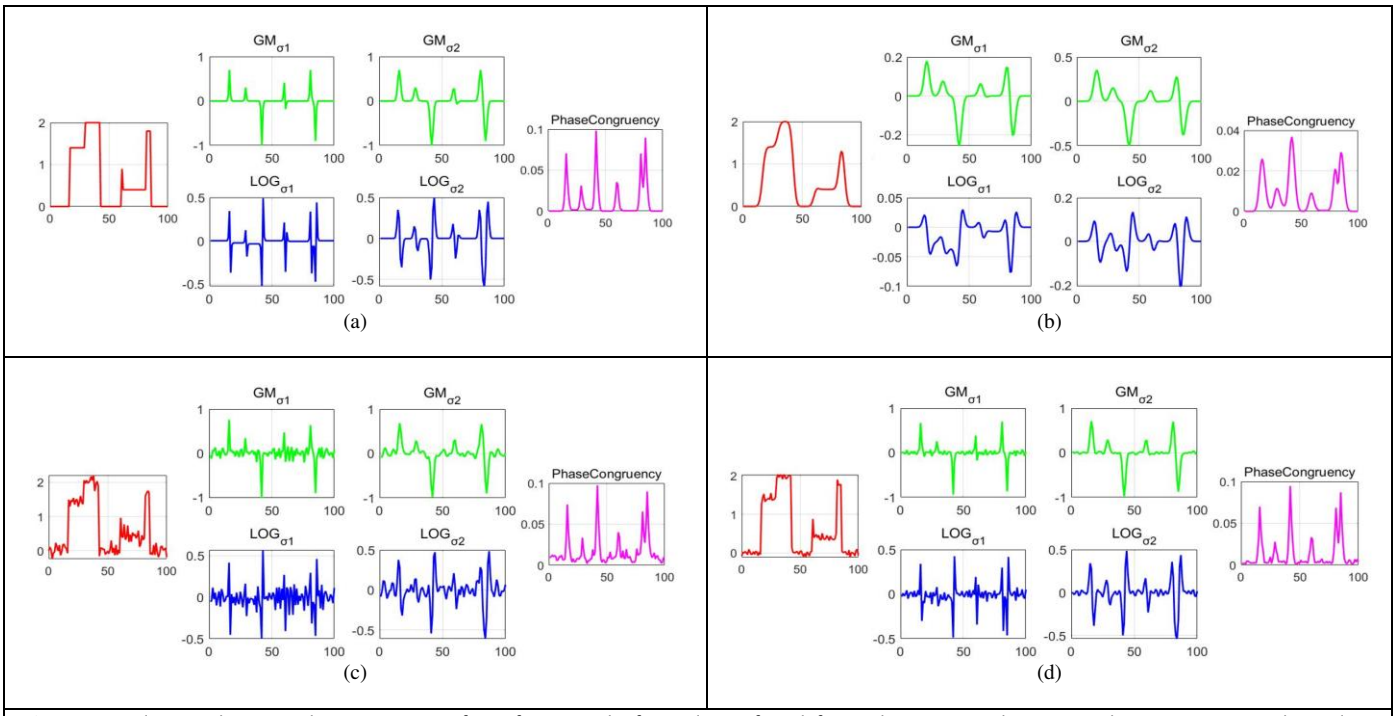

Figure 2. Analysis on the GM and LoG responses of step function. The four columns from left to right are: step edges, GM and LoG responses, and PC value. (a) Ideal edge. (b) Gaussian blur. (c) Gaussian noise. (d) DCT compression.

Figure 3 shows the PC map of reference image and its corresponding distorted images, compared with the GM and LoG filtered results. Note that the proposed PC is computed on small scales. In the reference image, PC map reflects the significance of local structures even if the local contrast is low, thus PC is able to capture more details of structural information than GM and LoG maps. For distorted images, PC map still shows more distorted structures than GM and LoG maps, regardless of distortion types. Especially, the distorted edges in JPEG image can be clearly sensed by PC map, but are hardly emerged by GM and LoG according to Figure 3. From the filtration results, the PC map has the ability to figure out edges more completely and clearly. This comparison proclaims that the PC map constructed by GM and LoG is an efficient feature map which contains enough structural distortion information to distinguish the faint features in distorted images, thus can be helpful to improve the prediction accuracy for image quality.

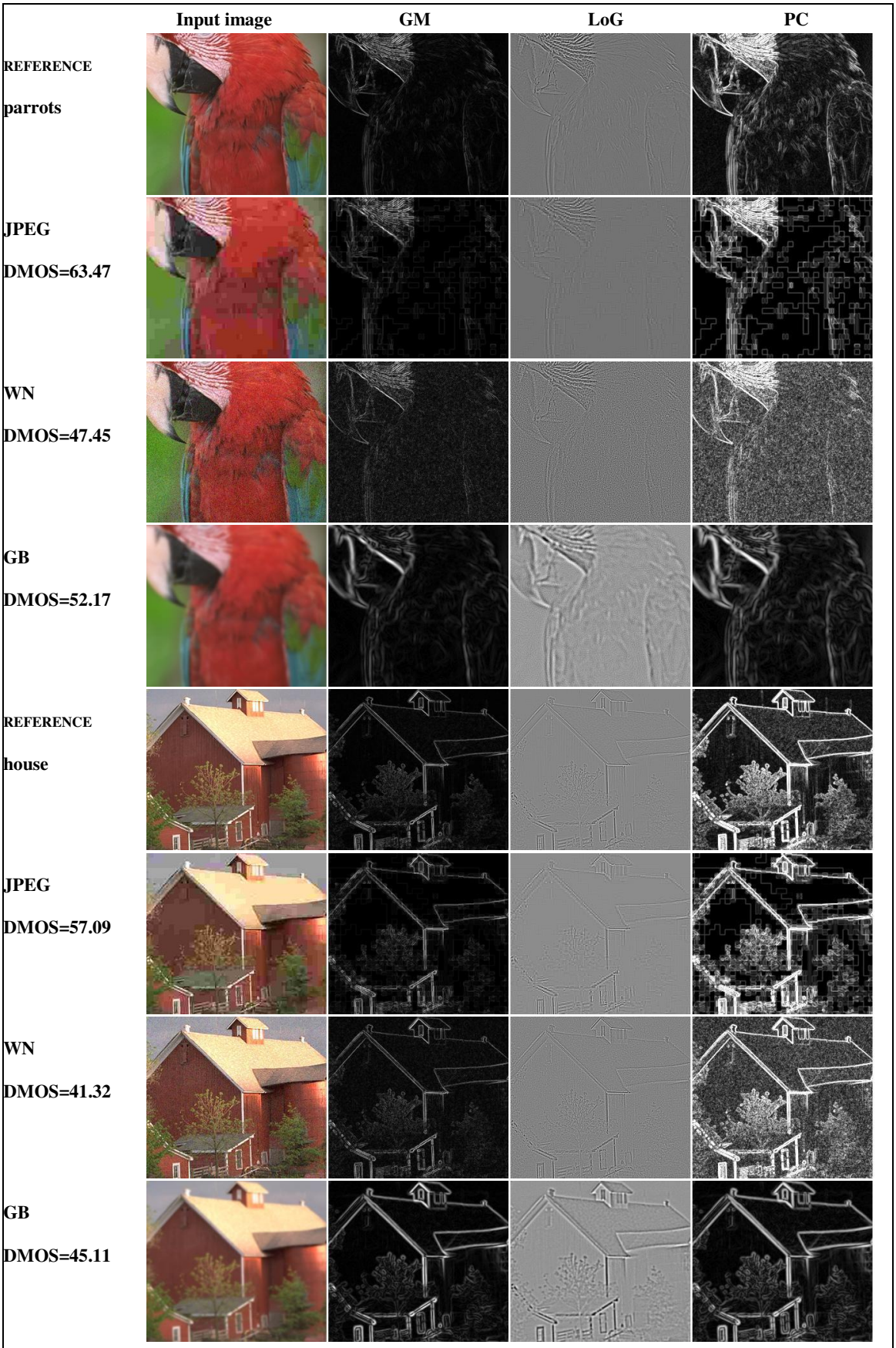

Figure 3. The PC map of reference image and its corresponding distorted images compared with GM and LoG maps.

2.2 FR-IQA model based on the proposed PC algorithm

Since the PC value represents the significance of edges, the quality map which measures local similarity of PC between signal $f_1(x)$ and $f_2(x)$ is defined as Eq. (19):

$$Q_{PC}(x,y) = \frac{2PC_1(x,y) \cdot PC_2(x,y) + c_1}{PC_1^2(x,y) + PC_2^2(x,y) + c_1} \tag{19}$$

where c_1 is a positive constant to prevent division by zero and increase the stability. This is a commonly applied measure to define the similarity of two positive real numbers 1, and the result of each image pixel ranges within (0, 1]. Higher result means higher similarity between distorted and reference images.

In order to yield the overall score of an image, the pixel based similarity map should be converted to a scalar score with a proper pooling method. Weighted pooling methods are widely discussed and many researches on pooling strategy have been done for image and video quality assessment [3, 43-46]. Average pooling is employed based on the hypothesis that each part of the image contributes the same importance in overall quality, which is the most commonly used method for pooling process. We compute the quality map with average pooling method as:

$$mean(Q_{PC}) = \frac{1}{N}\sum\nolimits_{x,y} Q_{PC}(x,y) \tag{20}$$

where *N* represents the number of pixels in test image.

For further comparison, we utilize a standard deviation pooling method which considers that different local structures suffer different degradations. It has been proved to be efficient for gradient similarity based IQA method in 13, thus we compute the standard deviation of the similarity map of PC as follow:

$$std(Q_{PC}) = \sqrt{\frac{1}{N}\sum\nolimits_{x,y} (Q_{PC}(x,y) - mean(Q_{PC}))^2} \tag{21}$$

The average pooling result gives higher score to better image quality since it measures the average similarity between distorted and reference images, whereas the standard deviation pooling gives higher score to lower image quality and larger distortion, on account of the ability to measure difference between distorted and reference images.

In order to adjust the curvature of the relation between predicted quality scores and subjective scores, we use a nonlinear transformation to calculate the score as follows:

$$q_m = [mean(Q_{PC}(x))]^{\frac{1}{3}} \tag{22}$$

$$q_{sd} = [std(Q_{PC}(x))]^{\frac{1}{3}} \tag{23}$$

Note that the transformation does not change the order of the estimated scores of distorted images, hence it has no influence in the evaluation of monotonicity.

2.3 Replace the PC computation in FSIM

FSIM metric [11] separated the feature similarity measurement between signal $f_1(x)$ and $f_2(x)$ into two components, each for PC or GM. The feature $S_L(x)$ combined PC with GM is defined as:

$$S_L(x) = S_{PC}(x)S_G(x) \tag{24}$$

where $S_G(x)$ is the similarity measure of image gradient. We replace the PC computation with our proposed PC metric, and compute the objective score in the way as the FSIM algorithm does:

$$S_{FSIM} = \frac{\sum_x S_L(x) \cdot PC_m(x)}{\sum_x PC_m(x)} \tag{25}$$

where

$$PC_m(x) = \max(PC_1(x), PC_2(x)) \tag{26}$$

We compared this result with the original FSIM performance to test the validity and accuracy of our computation to express the structural features as a phase congruency expression.

3. Experimental setup

We test the proposed FR-IQA model on three benchmark databases: LIVE [47], CSIQ [48], and TID2013 [49]. LIVE database contains 29 reference images and 779 distorted images generated with 5 distortions types: JPEG compression, JPEG2000 compression, white noise, Gaussian blur and simulated fast fading. CSIQ database consists of 30 reference images and 866 distorted images generated with 6 different distortions types: JPEG compression, JPEG2000 compression, additive white noise, additive pink Gaussian noise, Gaussian blur, and global contrast decrements. The Difference Mean Opinion Score (DMOS) values are provided in LIVE and CSIQ databases as the subjective score for distorted images, which is a positive score representing the degree of distortion from human evaluation. The TID2013 database is the largest of the three databases which contains 3000 distorted images created from 25 reference images with 24 types of distortions at 5 levels. The Mean Opinion Score (MOS) are provided as subjective score of human evaluation, which gives higher value to higher subjective image quality. The most

commonly applied methodology in evaluation of IQA models is the Spearman Rank Order Correlation Coefficient (SROCC). It takes consideration of prediction monotonicity, which is a typical aspect of IQA performance [50].

The SROCC between predicted score and reference subjective score is defined as:

$$SROCC(X,S) = 1 - \frac{6\sum_{i=1}^{n} d_i^2}{n(n^2-1)} \tag{27}$$

where X and S are the vectors of the predicted results and subjective scores of the test images, and d_i is the difference between the rank of an objective score in X and the rank of its corresponding subjective score in S.

The Pearson Linear Correlation Coefficient (PLCC) metric, which measures the prediction accuracy, should be applied after a nonlinear regression. A logistic function with an added linear term [51] is employed as follow:

$$X_r = \beta_1 \left(\frac{1}{2} - \frac{1}{1+\exp\left(\beta_2 (X-\beta_3)\right)} \right) + \beta_4 X + \beta_5 \tag{28}$$

where $\beta_i, i = 1, 2, \ldots, 5$, are parameters to be fitted in the regression function. X_r denotes the IQA scores after nonlinear regression. The PLCC is defined as:

$$PLCC(X_r,S) = \frac{\bar{X}_r^T \bar{S}}{\sqrt{\bar{X}_r^T \bar{X}_r \bar{S}^T \bar{S}}} \tag{29}$$

where $\bar{X}_r^T$ and $\bar{S}$ denote the vectors of scores with mean value removed.

The Root Mean Square Error (RMSE), which evaluates the prediction consistency of the IQA performance, is computed as:

$$RMSE(X_r,S) = \sqrt{(X_r - S)^T (X_r - S)/n} \tag{30}$$

In the computation stages of our experiment, the constant c_0 in divisive normalization by Eq. (11) and Eq. (12) is selected as 120, the standard deviation of the original multi-scale Gaussian functions we select are 0.3 and 0.6. The constant ε in PC calculation by Eq. (17) is selected as 25, and the constant c_1 in similarity map calculation by Eq. (18) is selected as 3×10^{-5}, which show the best property in the experimental performance of the proposed model. When replacing the PC algorithm in FSIM [11], we select the scale factor of Gaussian functions as 2 and 4, since the image gradient in FSIM is calculated by Prewitt operator with a small-scale window, thus the phase computation needs to catch structural information with a larger range. According to the scale of Gaussian function, the constant c_0 is adjusted to 60, ε is selected as 5.5, and c_1 is selected as 0.03.

4. Results and discussion

4.1 Experimental results on different databases

In order to validate the performance of the proposed metric, we investigate the model scores for images from the three benchmark databases, and compute the SROCC, PLCC, and RMSE between the model scores and subjective opinion scores provided by the databases as the performance criteria. The performances of proposed metric and competitors are shown in Table 1. On each database, the top three metrics are presented in boldface. The results of these comparison algorithms on the three major databases are provided by their authors in the original literatures, or computed by the downloadable source codes they provide on the internet. In Table 1, the result of standard deviation pooling method is much more efficient than the average pooling method. The proposed model with standard deviation pooling ranks 4th on LIVE database, 2nd on CSIQ, 1st on TID2013 database, and 1st on average across the three databases. Particularly, the proposed method performs significantly better than other metrics on TID2013 database. According to the experimental results, the proposed model shows stability and efficiency on a large range of different distortion types, since TID2013 is one of the most extensively used database which contains the most types of distortion and varies of image content.

Table 1 Performances of proposed metric and competitors on three benchmark databases in terms of SROCC, PLCC and RMSE. The top three values are shown in boldface for each database.

	PSNR	SSIM	MS-SSIM	IW-SSIM	RFSIM	IFC	VIF	FSIM	GMSD	mean(Q)	std(Q)
SROCC											
LIVE	0.8756	0.9479	0.9513	0.9567	0.9434	0.9259	**0.9636**	**0.9634**	**0.9603**	0.9508	0.9579
CSIQ	0.8058	0.8756	0.9133	0.9213	**0.9291**	0.7671	0.9195	0.9240	**0.9570**	0.9193	**0.9494**
TID2013	0.6394	0.7417	0.7859	0.7779	0.7743	0.5390	0.6770	**0.8022**	**0.8044**	0.7856	**0.8101**
Average	0.7100	0.8012	0.8374	0.8346	0.8317	0.6463	0.7703	**0.8519**	**0.8590**	0.8382	**0.8609**
PLCC											
LIVE	0.8723	0.9449	0.9489	0.9522	0.9386	0.9268	**0.9604**	**0.9597**	**0.9603**	0.9450	0.9534
CSIQ	0.7512	0.8613	0.8991	0.9144	0.9164	0.8366	**0.9277**	0.9118	**0.9541**	0.9006	**0.9453**
TID2013	0.7017	0.7895	0.8329	0.8319	0.8329	0.7220	0.7720	**0.8589**	**0.8590**	0.8290	**0.8746**
Average	0.7395	0.8289	0.8647	0.8675	0.8662	0.7777	0.8326	**0.8857**	**0.8937**	0.8618	**0.9010**
RMSE											
LIVE	13.3597	8.9455	8.6188	8.3472	9.4298	10.2641	**7.6137**	**7.6742**	**7.6214**	8.9335	8.2420
CSIQ	0.1733	0.1334	0.1149	0.1063	0.1051	0.1438	**0.0980**	0.1078	**0.0786**	0.1141	**0.0857**
TID2013	12.2420	10.5462	9.5098	9.5364	9.5089	11.8900	10.9215	**8.8004**	**8.7966**	9.6088	**8.3324**

In addition, the data of S_{FSIM} in Table 2 represents the result that we replace the PC algorithm in FSIM metric with our proposed PC metric, compared with the original FSIM results in terms of SROCC.

Table 2 Performance of S_{FSIM} in terms of SROCC, where the PC algorithm in FSIM metric has been replaced by the proposed PC algorithm.

	LIVE	CSIQ	TID2013	Weighted Average
FSIM	0.9634	0.9240	0.8022	0.8519
S_{FSIM}	0.9628	0.9262	0.8056	0.8544

It is shown that the performance of S_{FSIM} on the three databases is very close to the FSIM method, and the result has been slightly improved on CSIQ and TID2013 databases. In fact, the proposed PC method reduces the computational complexity and shows better performance in average than the original PC algorithm. Such result validated that our PC calculation method is effective for phase information representation compared with traditional PC method. The computational PC model constructed from GM and LoG maps works stably as a phase-based mechanism without calculating the phase information directly from the multi-scale frequency domain.

Figure 4 shows the scatter plots of predicted quality scores versus subjective scores of proposed model, compared with other metrics on LIVE database. The horizontal axis denotes the objective scores computed by different IQA metrics, while the vertical axis denotes the DMOS values. In this figure, we can see the monotonicity and consistency of the proposed and comparison IQA metrics more intuitively, since the scatter plots reflects the relationship between objective and subjective evaluations by pairs of coordinates.

4.2 Experimental results on individual distortion types

For further comparison of the performance between the proposed model and competitors, we present the performance of proposed model and comparison metrics on each individual distortion type in terms of SROCC in Table 3. For each distortion type, the top three algorithms are presented in boldface. The last row counts the number of times that each algorithm reaches the top three across all distortion types.

According to the table, the proposed model with standard deviation pooling works stably and robustly on most distortion types across the three databases, and finally reaches the highest hit number compared with all the competitors. Particularly, it performs better on the distortion types where structural changes occurs rather than contrast and intensity changes, since the PC operator is to measure how salient is the edge.

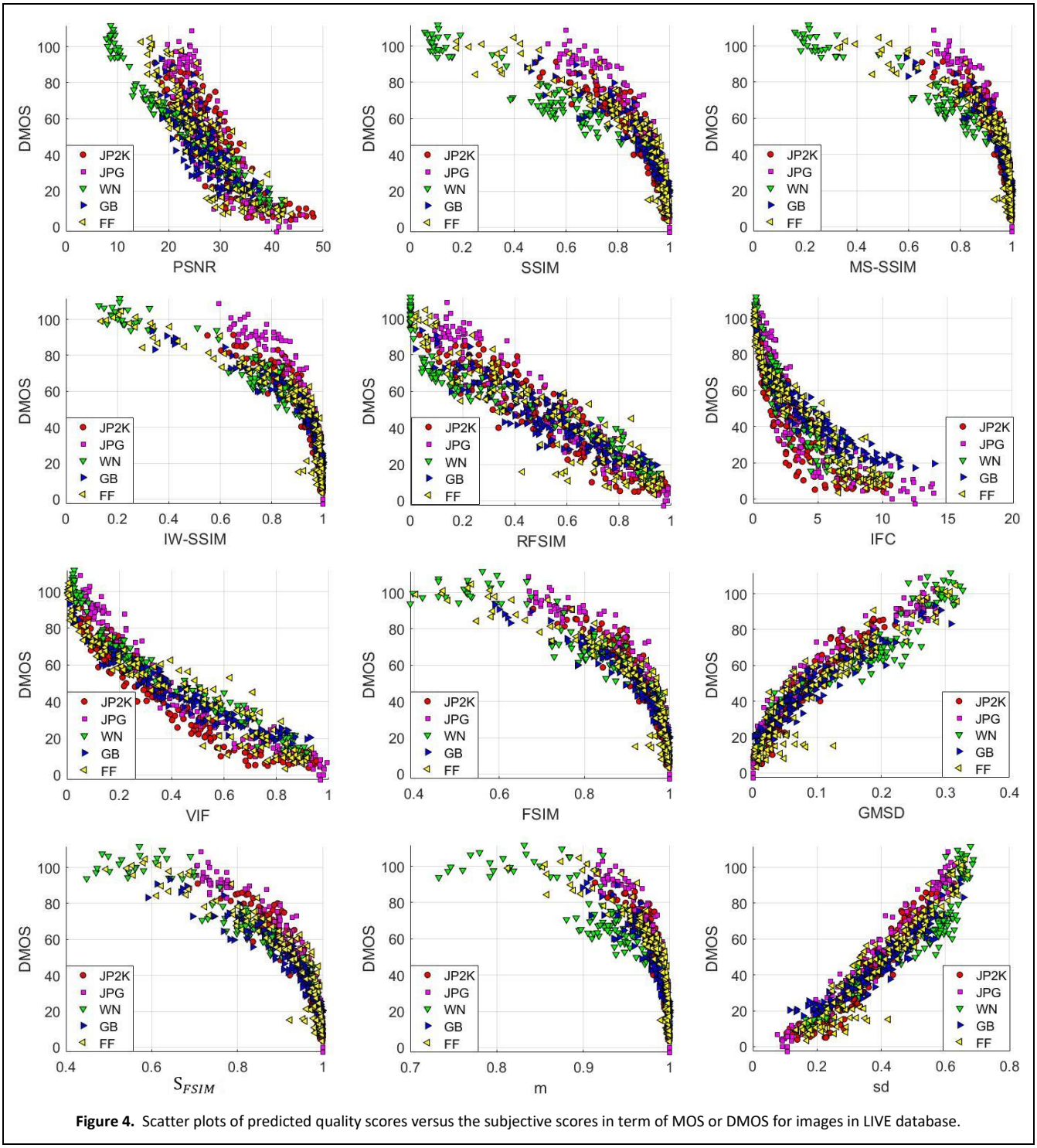

Figure 4. Scatter plots of predicted quality scores versus the subjective scores in term of MOS or DMOS for images in LIVE database.

4.3 Comparison of running time

Since the computational efficiency plays an important role in practical applications, it is necessary to improve the operation speed and efficiency of IQA metrics. In Table 4, we present the running time of the proposed method and 9 competing FR-IQA models on each 512×512 image in average. Particularly, the running time of S_{FSIM} represents the result that we replace the PC algorithm in

FSIM metric. We tested the algorithms using MATLAB R2019a, and the source codes of the competitors were originally reported by their authors. The experiments were operated on a personal desktop computer with Intel Core i5-6400 CPU @2.7GHz and 8G RAM.

Table 3 Performances of proposed metric and competitors on each individual distortion type in terms of SROCC. The top three algorithms are presented in boldface for each distortion type.

	Distortion	PSNR	SSIM	MS-SSIM	IW-SSIM	RFSIM	IFC	VIF	FSIM	GMSD	mean(Q)	std(Q)
LIVE	JP2K	0.8954	0.9614	0.9654	0.9653	0.9379	0.9100	0.9683	**0.9717**	**0.9711**	0.9672	**0.9707**
	JPEG	0.8809	0.9764	0.9793	**0.9809**	0.9612	0.9440	**0.9842**	**0.9834**	0.9782	0.9801	0.9797
	WN	**0.9854**	0.9694	0.9731	0.9671	**0.9800**	0.9377	**0.9845**	0.9652	0.9737	0.9494	0.9624
	GB	0.7823	0.9517	0.9584	**0.9722**	0.9201	0.9649	**0.9722**	**0.9708**	0.9567	0.9539	0.9662
	FF	0.8907	0.9556	0.9321	0.9443	0.9269	**0.9644**	**0.9652**	0.9499	0.9416	0.9558	**0.9578**
CSIQ	AWN	0.9363	0.8974	0.9471	0.9377	0.9402	0.8460	**0.9571**	0.9262	**0.9676**	0.9507	**0.9637**
	JPEG	0.8882	0.9546	0.9622	**0.9664**	0.9481	0.9395	**0.9705**	**0.9654**	0.9651	0.9603	0.9652
	JP2K	0.9363	09606	**0.9691**	0.9681	0.9635	0.9262	0.9672	0.9685	**0.9717**	0.9577	**0.9715**
	PGN	0.9338	0.8922	0.9330	0.9057	0.9357	0.8279	**0.9509**	0.9234	**0.9502**	0.9317	**0.9432**
	GB	0.9289	0.9609	0.9720	**0.9781**	0.9607	0.9593	**0.9747**	**0.9729**	0.9712	0.9535	0.9710
	Contrast	0.8622	0.7922	**0.9521**	**0.9540**	**0.9526**	0.5416	0.9361	0.9420	0.9040	0.9368	0.9374
TID2013	AWGN	**0.9291**	0.8671	0.8645	0.8438	0.8862	0.6611	0.8994	0.8973	**0.9462**	0.9033	**0.9352**
	ANMC	**0.8984**	0.7726	0.7729	0.7514	0.8447	0.5351	0.8299	0.8207	**0.8684**	0.8276	**0.8555**
	SCN	**0.9198**	0.8515	0.8543	0.8166	0.8791	0.6601	0.8834	0.8749	**0.9350**	0.8846	**0.9251**
	MN	0.5416	0.7767	0.8014	0.8063	**0.8415**	0.6732	**0.8642**	**0.8013**	0.7075	0.7937	0.7547
	HFN	**0.9141**	0.8634	0.8603	0.8553	**0.9135**	0.7405	0.8972	0.8983	**0.9162**	0.8879	0.9071
	IMN	**0.8968**	0.7503	0.7628	0.7281	**0.9065**	0.6407	**0.8536**	0.8072	0.7637	0.7893	0.7236
	QN	0.8808	0.8657	0.8705	0.8467	**0.8950**	0.6282	0.7853	0.8719	**0.9049**	0.8606	**0.9013**
	GB	0.9149	0.9667	0.9672	**0.9701**	**0.9689**	0.8906	0.9649	0.9550	0.9113	**0.9675**	0.9521
	DEN	**0.9480**	0.9254	0.9267	0.9152	0.9346	0.7779	0.8910	0.9301	**0.9525**	0.9317	**0.9440**
	JPEG	0.9189	0.9200	0.9265	0.9186	**0.9381**	0.8356	0.9191	0.9324	**0.9507**	0.9351	**0.9467**
	JP2K	0.8840	0.9468	0.9504	0.9506	0.9508	0.9077	0.9516	**0.9576**	**0.9657**	0.9569	**0.9626**
	JGTE	0.7685	**0.8493**	0.8475	0.8387	0.8337	0.7425	0.8409	0.8463	0.8403	**0.8647**	**0.8600**
	J2TE	0.8883	0.8828	0.8888	0.8656	**0.9069**	0.7769	0.8760	0.8912	**0.9136**	0.9007	**0.9078**
	NEPN	0.6860	0.7821	0.7968	0.8010	0.7716	0.5736	0.7719	0.7917	**0.8140**	**0.8055**	**0.8258**
	Block	0.1552	0.5720	0.4800	0.3716	0.0349	0.2413	0.5306	0.5489	**0.6625**	**0.6480**	**0.6638**
	Mean shift	0.7672	**0.7752**	**0.7906**	**0.7833**	0.5497	0.5522	0.6275	0.7530	0.7351	0.7180	0.7162
	Contrast	0.4403	0.3775	0.4633	0.4592	0.3995	-0.180	**0.8385**	**0.4686**	0.3235	**0.4843**	0.3256
	CCS	**0.0944**	-0.414	-0.410	-0.420	**-0.017**	-0.403	-0.310	**-0.275**	-0.295	-0.396	-0.316
	MGN	**0.8905**	0.7803	0.7785	0.7727	0.8451	0.6142	0.8468	0.8469	**0.8886**	0.8189	**0.8612**
	CN	0.8411	0.8566	0.8527	0.8761	0.8914	0.8160	0.8946	**0.9120**	**0.9298**	0.8928	**0.9206**
	LCN	0.9145	0.9057	0.9067	0.9037	0.8982	0.8180	0.9203	**0.9466**	**0.9629**	0.9416	**0.9630**
	CQD	**0.9269**	0.8542	0.8554	0.8401	0.8953	0.6006	0.8414	0.8759	**0.9102**	0.8867	**0.9059**
	Chr. abr.	**0.8873**	0.8775	0.8784	0.8681	**0.8987**	0.8209	**0.8848**	0.8714	0.8530	0.8755	0.8496
	Sampling	0.9042	0.9461	0.9482	0.9474	0.9318	0.8884	0.9352	0.9565	**0.9683**	**0.9569**	**0.9629**
Hit number		11	2	3	7	11	1	**12**	11	**20**	6	**21**

Table 4 Running time of the proposed PC based model and the competitors

Models	Running time (s)
VIF	0.7677
IFC	0.7574
IW-SSIM	0.3590
FSIM	0.1818
RFSIM	0.0707
S_{FSIM}	0.0488
MS-SSIM	0.0473
std(Q)	0.0338
SSIM	0.0209
GMSD	0.0137
PSNR	0.0104

According to the comparison, PSNR, GMSD and SSIM are the three fastest metrics owing to the low computational complexities, while the proposed std(Q) model ranks the 4th, since phase computation needs multi-scale calculation. The proposed PC based model runs 5.38 times faster than FSIM, 10.62 times faster than IW-SSIM, and 22.71 times faster than VIF. In particular, when replacing the PC computation in FSIM with the proposed PC algorithm, the code runs 3.73 times faster than the original FSIM model, which validated that the proposed PC based on derivatives of Gaussian function is more efficient and less complex in computation than traditional PC method. This is mostly because of the simplicity of the computation on Gaussian function and the non-directional features generated by Gaussian-based atoms, which shows less complexity compared with the Gabor-based features.

5. Conclusion

In this paper, we proposed a novel algorithm of phase congruency map computation to represent quality-aware structural information of image, and then proposed an FR-IQA model based on the quality feature, which we proved to be quality aware. Instead of traditional multiscale log-Gabor filters with multi-orientations, we utilized image gradient magnitude and Laplacian of Gaussian filters, which are the first-order and the second-order derivatives of Gaussian function, to generate the odd-symmetric and even-symmetric components of an image when computing the dimensionless phase congruency index. This calculation with Gaussian based filters is much simpler in computation and more concise than traditional PC algorithm with log-Gabor filters, In this study we have validated that this phase congruency map contains enough structural information and can extract faint features

such as the edges, lines, corners, and other local structures from both reference and distorted images, which makes it available to measure the degree of distortions.

The experimental results have indicated that the proposed method performs consistently and stably on different distortion types across three benchmark databases, while it costs less time to achieve in computational process compared with other outstanding metrics. Especially, the experiment on FSIM metric where we replaced the original PC algorithm with the proposed PC feature map shows that the first-order and second-order derivatives of Gaussian function can efficiently construct a new PC feature map. Meanwhile, with performing similarly in prediction results but much faster in running time compared with conventional PC algorithms, the proposed PC shows to be a state-of-the-art feature map for IQA model design.

Although the proposed model works slightly better than GMSD, the PC feature based on Gaussian derivatives actually reflect the characteristics of image information where image components in different frequencies show similar responses in phase. Therefore, PC feature detects structural information at all kinds of phase angles, whereas image gradient mostly focuses on step features with a phase angle of 0 or 180 degrees. Despite that the gradient map in the proposed feature resembles the gradient magnitude in GMSD and FSIM, Gaussian derivatives are strictly circular symmetric filters, which are different from Prewitt or Sobel operator. Because of the non-directional properties and the ability to reflect image information in both odd and even phases, the proposed PC feature is expected to play an important role in image enhancement applications based on IQA features.

In conclusion, this paper has proposed an efficient PC feature map based on derivatives of non-directional Gaussian function. This symmetric operator is proved to be quality aware and works stably in the proposed FR model with reduction in running time compared with conventional PC metrics. Therefore, the proposed feature map can play an important role in the image quality related applications in the future research.

Abbreviations

FR: full reference; GM: gradient magnitude; IQA: image quality assessment; LoG: Laplacian of Gaussian; MSE: mean squared error; PC: phase congruency; PLCC: Pearson Linear Correlation Coefficient; PSNR: peak signal-to-noise ratio; SROCC: Spearman rank order correlation coefficient.

Availability of data and materials

The source code is available from the authors on reasonable request.

Competing interests

The authors declare that they have no competing interests.

Funding

This work is supported by the National Natural Science Foundation of China (NSFC, No. 62071375).

Author contributions

Both authors have made contributions to this manuscript. CC: software simulations, experimental analysis, original draft writing. XM: research plan designing, methodology, draft revising.

Acknowledgements

Not applicable.

Author information

Congmin Chen received the B.Sc. degree in information engineering from the School of Electronic and Information Engineering, Xi'an Jiaotong University, Xi'an, Shaanxi, China, in 2012. She is currently pursuing the Ph.D. degree with the Institute of Image Processing and Pattern Recognition, Xi'an Jiaotong University. Her research interest focuses on visual quality perception.

Dr. **Xuanqin Mou** has been with the Institute of Image Processing and Pattern Recognition (IPPR), Electronic and Information Engineering School, Xi'an Jiaotong University, Xi'an, China, since 1987, where he has been an Associate Professor since 1997, and a Professor since 2002. He is currently the Director of IPPR and the director of the National Data Broadcasting Engineering and Technology Research Center. He served as a member of the 12th Expert Evaluation Committee for the National Natural Science Foundation of China. He now serves for the Executive Committee of the China Society of Image and Graphics, the executive committee of the Chinese Society for Stereology. He has authored or co-authored over 200 peer-reviewed journal or conference papers. He was a recipient of the Yung Wing Award for Excellence in Education, the KC Wong Education Award. He received a Second-class Award for Invention by the Ministry of Education of China as principle investigator, and a Technology Academy Awards from the Government of Shaanxi Province, China.

References

1. Z. Wang, A. C. Bovik and H. R. Sheikh, and E. P. Simoncelli, Image quality assessment: from error visibility to structural similarity. IEEE Trans. Image Process., vol. 13, no. 4, pp. 600-612, Apr. 2004.
2. Z. Wang, E. P. Simoncelli, and A. C. Bovik, Multiscale structural similarity for image quality assessment. Proc. IEEE 37th Conf. Rec. Asilomar Conf. Signals, Syst. Comput., vol. 2, Nov. 2003, pp. 1398-1402.
3. Z. Wang, and Q. Li, Information content weighting for perceptual image quality assessment. *IEEE Trans. Image Process.*, vol. 20, no. 5, pp. 1185-1198, May 2011.
4. L. Zhang, L. Zhang, and X. Mou, RFSIM: a feature based image quality assessment metric using Riesz transforms. *Proc. IEEE Int. Conf. on Image Process.*, 2010, Hong Kong.
5. L. Zhang, H. Li, SR-SIM: A fast and high performance IQA index based on spectral residual. *IEEE Int. Conf. on Image Process.*, pp. 1473–1476, 2013.
6. H. R. Sheikh, A. C. Bovik and G. de Veciana, An information fidelity criterion for image quality assessment using natural scene statistics. *IEEE Trans. Image Process.*, vol.14, no.12, pp. 2117- 2128, Dec. 2005.
7. H. R. Sheikh, and A.C. Bovik, Image information and visual quality. *IEEE Trans. Image Process.*, vol.15, no.2, pp. 430- 444, Feb. 2006.
8. D. Marr, *Vision*. New York: W. H. Freeman and Company, 1980.
9. D. Marr and E. Hildreth, Theory of edge detection. *Proc. R. Soc. Lond. B*, vol. 207, no. 1167, pp. 187-217, Feb. 1980.
10. M.C. Morrone and D.C. Burr, Feature detection in human vision: a phase-dependent energy model. *Proc. R. Soc. Lond. B*, vol. 235, no. 1280, pp. 221-245, Dec. 1988.
11. L. Zhang, L. Zhang, X. Mou and D. Zhang, FSIM: a feature similarity index for image quality assessment. *IEEE Trans. Image Process.*, vol. 20, no. 8, pp. 2378-2386, Aug. 2011.
12. A. Liu, W. Lin, M. Narwaria, Image quality assessment based on gradient similarity. *IEEE Trans. Image Process.*, vol. 21, no. 4, pp. 1500–1512, 2012.
13. W. Xue, L. Zhang, X. Mou, et al. Gradient magnitude similarity deviation: a highly efficient perceptual image quality index. *IEEE Trans. Image Process.*, vol. 23, no. 2, pp. 684-695, Feb. 2014.
14. E. P. Simoncelli, B. A. Olshausen, Natural image statistics and neural representation. *Annu. Rev. Neurosci*, 24:1193-216, 2001.
15. L. J. Croner and E. Kaplan, Receptive Fields of P and M Ganglion Cells Across the Primate Retina. *Vision Research*, vol. 35, no. 1, pp. 7-24, 1995.
16. M. Zhang, X. Mou, and L. Zhang, Non-shift edge based ratio (NSER): an image quality assessment metric based on early vision features. *IEEE Signal Process. Lett.*, vol. 18, no. 5, pp. 315-318, 2011.
17. W. Xue and X. Mou, Image quality assessment with mean squared error in a log based perceptual response domain. *Signal and Information Processing (ChinaSIP)*, 2014 IEEE China Summit & International Conference on IEEE, pp. 315-319, 2014.
18. X. Mou, W. Xue, C. Chen, and L. Zhang, LoG acts as a good feature in the task of image quality assessment. *Proc. IS&T/SPIE Electronic Imaging*, vol. 9023, California, USA, 2014.
19. X. Mou, W. Xue, and L. Zhang, Reduced reference image quality assessment via sub-image similarity based redundancy measurement. *Proc. IS&T/SPIE Electronic Imaging*, vol. 8291, California, USA, 2012.
20. Y. Chen, W. Xue, and X. Mou, Reduced-reference image quality assessment based on statistics of edge patterns. *Proc. IS&T/SPIE Electronic Imaging*, vol. 8299, California, USA, 2012.
21. C. Chen, and X. Mou, A Reduced-Reference Image Quality Assessment Model Based on Joint-Distribution of Neighboring LOG Signals. *Proc. IS&T Electronic Imaging*, vol. 18, pp. 1-8, 2016.

22. W. Xue, X. Mou, L. Zhang, and A. C. Bovik, Blind image quality assessment using joint statistics of gradient magnitude and Laplacian features. *IEEE Trans. Image Process.*, vol. 23, no. 11, pp. 4850-4862, 2014.

23. H.R. Sheikh, M.F. Sabir, A.C. Bovik, A statistical evaluation of recent full reference image quality assessment algorithms. *IEEE Trans. Image Process*., vol. 15, no. 11, pp. 3440–3451, 2006.

24. L. Zhang, L. Zhang, X. Mou, and D. Zhang, A comprehensive evaluation of full reference image quality assessment algorithms. *Proc. 19th IEEE ICIP*, Oct. 2012, pp. 1477–1480.

25. S. Athar, and Z. Wang, A comprehensive performance evaluation of image quality assessment algorithms. *IEEE Access*, vol. 7, pp. 140030-140070, 2019.

26. V. Domonkos. A comprehensive evaluation of full-reference image quality assessment algorithms on KADID-10k, 2019. [Online]. Available: http://arxiv.org/abs/1907.02096

27. J. Kim, H. Zeng, D. Ghadiyaram, et al. Deep Convolutional Neural Models for Picture-Quality Prediction. *IEEE Signal Processing Magazine*, vol. 34, no. 6, pp. 130-141, 2017.

28. S. Bosse, D. Maniry, K. Muller, et al. Deep Neural Networks for No-Reference and Full-Reference Image Quality Assessment. *IEEE Trans. Image Process.*, vol. 27, no. 1, pp. 206-219, 2018.

29. J. Kim, and S. Lee, Deep Learning of Human Visual Sensitivity in Image Quality Assessment Framework. *30th IEEE/CVF Conference on Computer Vision and Pattern Recognition* (CVPR), pp. 1969-1977, 2017.

30. D. Pan, P. Shi, M. Hou, et al. Blind Predicting Similar Quality Map for Image Quality Assessment. *31st IEEE/CVF Conference on Computer Vision and Pattern Recognition* (CVPR), pp. 6373-6382, 2018.

31. K. Lin, and G. Wang, Hallucinated-IQA: No-Reference Image Quality Assessment via Adversarial Learning. *31st IEEE/CVF Conference on Computer Vision and Pattern Recognition* (CVPR), pp. 732-741, 2018.

32. A.V. Oppenheim, and J.S. Lim, The importance of phase in signals. *Proc. of IEEE*, vol. 69, no. 5, pp. 529–541, 1981.

33. M.C. Morrone, J. Ross, D.C. Burr, and R. Owens, Mach bands are phase dependent. *Nature*, 324 (6049): 250–253, 1986.

34. M.C. Morrone, and R.A. Owens, Feature detection from local energy. *Pattern Recognit. Lett*. 6 (5): 303–313, 1987.

35. L. Henriksson, A. Hyvärinen, and S. Vanni, Representation of cross-frequency spatial phase relationships in human visual cortex. *J. Neuroscience*, vol. 29, no. 45, pp. 14342-14351, Nov. 2009.

36. P. Kovesi, Image features from phase congruency. *Videre: J. Comp. Vis. Res.*, vol. 1, no. 3, pp. 1-26, 1999.

37. P. Kovesi, Phase congruency: a low-level image invariant. *Psychological Res.*, vol. 64, no. 2, pp. 136-148, 2000.

38. D. Gabor, Theory of communication. *J. Inst. Elec. Eng.*, vol. 93, no. III, pp. 429-457, 1946.

39. D. J. Field, Relations between the statistics of natural images and the response properties of cortical cells. *J. Opt. Soc. Am. A*, vol. 4, no. 12, pp. 2379-2394, Dec. 1987.

40. L. Zhang, B. Li, L. Tian, W. Zhu, LPPCO: A novel multimodal medical image registration using new feature descriptor based on the local phase and phase congruency of different orientations. *IEEE Access,* vol. 6, pp. 71976–71987, 2018.

41. X. Miao, H. Chu, H. Liu, Y. Yang, and X. Li, Quality assessment of images with multiple distortions based on phase congruency and gradient magnitude. *Signal Process., Image Commun.*, vol. 79, pp. 54-62, Nov. 2019.

42. F. Zhang, B. Zhang, R. Zhang, and X. Zhang, SPCM: image quality assessment based on symmetry phase congruency. *Applied Soft Computing Journal*, vol. 87, Feb. 2020.

43. C. F. Li and A. C. Bovik, Content-partitioned structural similarity index for image quality assessment. *Signal Process., Image Commun.*, vol. 25, no. 7, pp. 517–526, Aug. 2010.

44. Z. Wang and X. Shang, Spatial pooling strategies for perceptual image quality assessment. *IEEE Int. Conf. Image Process.*, Sep. 2006, pp. 2945–2948.

45. A.K. Moorthy and A.C. Bovik, Visual importance pooling for image quality assessment. *IEEE J. Special Topics Signal Process*, vol. 3, pp. 193-201, April 2009.

46. J. Park, K. Seshadrinathan, S. Lee and A.C. Bovik, VQpooling: Video quality pooling adaptive to perceptual distortion severity. *IEEE Transactions on Image Processing*, vol. 22, no. 2, pp. 610-620, February 2013.

47. H. R. Sheikh, Z. Wang, L. Cormack, and A. C. Bovik. (2005) Live Image Quality Assessment Database Release 2. [Online]. Available: http://live.ece.utexas.edu/research/quality

48. E. C. Larson and D. M. Chandler, Most apparent distortion: full-reference image quality assessment and the role of strategy. *Journal of Electronic Imaging*, 19 (1), March 2010.

49. N. Ponomarenko, O. Ieremeiev, V. Lukin, K. Egiazarian, L. Jin, J. Astola, B. Vozel, K. Chehdi, M. Carli, F. Battisti, and C.-C. Jay Kuo, Color Image Database TID2013: Peculiarities and Preliminary Results. *Proc. of 4th Euro. Workshop on Vis. Inf. Process.*, pp. 106-111, Paris, France, 2013.

50. Final Report from the Video Quality Experts Group on the Validation of Objective Models of Video Quality Assessment, Phase II VQEG, Aug. 2003. [Online]. Available: http://www.vqeg.org/

51. H. R. Sheikh, M. F. Sabir, and A. C. Bovik, A statistical evaluation of recent full reference image quality assessment algorithms. *IEEE Trans. Image Process.*, vol. 15, no. 11, pp. 3440–3451, Nov. 2006.